# Synthesis of High-purity $Fe_2AlB_2$ and the Effect as Sintering Additive for $ZrB_2$①

WANG Rui[a, b] XU Wen-Tao[b] QIN Zi-Xuan[b, c]
LING Jun-Rong[b, c] ZHOU You-Fu[b②]

[a] (*Fujian Normal University, College of Chemistry and Materials Science, Fuzhou* 350007, *China*)
[b] (*Key Laboratory of Optoelectronic Materials Chemistry and Physics, Fujian Institute of Research on the Structure of Matter, Chinese Academy of Sciences, Fuzhou* 350002, *China*)
[c] (*University of Chinese Academy of Sciences, Beijing* 100039, *China*)

**ABSTRACT** $Fe_2AlB_2$ powder material was prepared by the direct reaction of iron, aluminum and boron powders in a tubular furnace. The effects of different Al contents, temperature and raw material pretreatment on the purity of product were studied. The mixed powder with the stoichiometric ratio of 1.5Al/2Fe/2B was processed by CIP (Cold Isostatic Pressing), and then calcined at 1150 ℃ for 120 min. The product containing a small amount of impurities is treated with alkaline solution to obtain high-purity $Fe_2AlB_2$ powder. $ZrB_2$-$Fe_2AlB_2$ composite ceramic was successfully prepared at 1250 ℃ by hot pressing sintering. The density, hardness and fracture toughness were 96.2%, 22 ±0.3 GPa and 5.78 ±0.5 MPa $m^{1/2}$, respectively.

**Keywords: MAB phase, ternary layered structure, high purity, $ZrB_2$;**
**DOI: 10.14102/j.cnki.0254–5861.2011–2882**

## 1 INTRODUCTION

Binary borides have excellent properties such as high temperature resistance, corrosion resistance and good chemical stability, which enable them to be high-temperature materials[1, 2]. However, due to their inherent brittleness, the application of binary borides is greatly restricted[3-5]. In recent years, with the development of MAX phase materials, the preparation of ternary-layered borides (MAB) has aroused a lot of interest[6]. For the MAX materials, M and A represent the transition metal and the third or fourth main group element (usually referring to Al or Si) respectively, while X is a carbon or nitrogen atom[7, 8]. MAB is similar, where B exclusively refers to boron element. The MAB material is a class of ternary transition metal (M) borides with atomic lamination, in which the metal-boride (M–B) layer composed of coplanar $BM_6$ triangular prisms is separated by single or double Al atomic layers[9-12]. Due to its special crystal structure, MAB material possesses integrated characteristics of metal and ceramic simultaneously, including good electrical conductivity, thermal conductivity[9, 10], high damage tolerance[11] and mechanical processability[12]. $Fe_2AlB_2$ is one of the most important MAB materials, of which the raw materials are quite accessible.

At present, $Fe_2AlB_2$ is mainly synthesized by hot pressing or arc-melting method, which is complicated and expensive. The as-product is in bulk state leading to low purity, which hinders its research and application. To develop the method of large-scale production of high-purity $Fe_2AlB_2$, a simple solid-state synthesis was investigated in this work. In addition, the weak bonding between adjacent layers of metal boride and Al in $Fe_2AlB_2$ could yield Al and FeB *in situ* at relatively high temperature. Zirconium diboride ($ZrB_2$) has attracted more attention due to wide-range applications such as high temperature structural ceramics, cutting tools and wear-resistant parts, but it is difficult to obtain high density

Received 19 May 2020; accepted 10 October 2020
① This work was supported by the grants of CAS Priority Research Program (XDB20010300, XDA21010204) and Science and Technology Program of Fujian Province (2017T3001)
② Corresponding author. E-mail: yfzhou@fjirsm.ac.cn

even under extremely high sintering temperature (~2000 ℃) with outer pressure as assistance. The *in-situ* liquid Al from decomposition of $Fe_2AlB_2$ has good wettability, which can accelerate mass transfer, remove the oxides from the surface of $ZrB_2$ (such as $ZrO_2$, $B_2O_3$ or amorphous Zr–B–C–O) and promote densification. Meanwhile, the produced FeB has good compatibility with the $ZrB_2$ matrix. Herein, the sintering of $ZrB_2$ with $Fe_2AlB_2$ additive was performed to obtain highly dense ceramic materials for the first time.

## 2 EXPERIMENTAL

### 2. 1 Preparation of $Fe_2AlB_2$ powder

Commercially available Al (99.99%, 3$\mu$m), Fe (99.99%, 3$\mu$m) and B (≥95%, 5$\mu$m) powders (Aladdin Chemical Co., China) were used as received. In a typical synthesis, raw materials were accurately weighed according to a certain ratio, and mixed via ball milling at 250 rpm for 24 hours. After drying and sieving, the obtained powder was uniaxially pressed into a disk of 30 mm diameter and 4 mm thickness, and then cold isostatically pressed under 150 MPa. The green body was placed in a BN crucible and heated in a tube furnace from 1130 to 1170 ℃ for different duration time. As a comparison, the parallel preparation was also carried out without cold isostatic pressing. The product was crushed in the agate mortar and soaked in HCl/NaOH solution under ultrasonic stirring for purification. Finally, the obtained powder was washed and collected by filtration.

### 2. 2 Sintering of $ZrB_2$ ceramic with $Fe_2AlB_2$ additive

$ZrB_2$ (99.99%, 3 $\mu$m, Aladdin Chemical Co., China) and different contents (25, 30 and 35 wt%) of $Fe_2AlB_2$ were mixed by ball-milling in ethanol media for 24 h at 250 rpm. The slurry was dried at 80 ℃ and screened through a 150-mesh sieve. The powder mixture was compacted in a graphite die with the diameter of 25 mm and hot pressing sintered under a pressure of 35 MPa at different temperature for 120 min in Ar atmosphere.

### 2. 3 Characterization

The phase compositions were examined by powder X-ray diffraction (XRD, Mini Flex600, Rigaku, Japan) using Cu$K\alpha$ radiation with a scan step width of 0.02 °. Calc. $Fe_2AlB_2$ refers to the theoretical diffraction pattern derived from the result of crystal simulation. The microstructures were investigated using a scanning electron microscope (SEM, Sigma300, Carl Zeiss Microscopy Ltd, Germany and Su-8010, Hitachi, Japan). The density was measured by the Archimedes method. Vickers hardness (HV) was measured under the loads of 9.8 N for 15s on a polished surface. The direct crack measurement (DCM) method was used to evaluate fracture toughness, based on an equation suitable for the ratio of crack length to diagonal length larger than 2[13]. Thermogravimetric analysis (TGA, STA 449F3, Netzsch, Germany) was performed in $N_2$ atmosphere at a heating rate of 10 ℃/min.

## 3 RESULTS AND DISCUSSIONS

### 3. 1 Characterization of $Fe_2AlB_2$ powder

The phase composition of product was characterized by XRD analysis. As shown in Fig. 1, $Fe_2AlB_2$ is the predominant phase with the trace of FeB, $Al_2O_3$ and $Al_{13}Fe_4$ after being calcined at 1130 ℃. It has been widely recognized that excess Al is necessary to achieve high conversion of MAB phase, considering the volatilization of Al at high temperature. The formation of FeB impurity was suppressed by increasing Al content. For the product with the Al ratio of 1.7, FeB has been completely eliminated. Meanwhile, the unwanted Al-rich intermetallic, identified as $Al_{13}Fe_4$, is difficult to avoid. The Al element evaporated during the sintering process at high temperature. Aluminum is liable to react with oxygen even at extremely low oxygen partial. The existence of $Al_2O_3$ originates from the oxide on the surface of Al powder or the aluminothermic reduction of oxide in other reagents. Fortunately, the above two byproducts can be easily removed by treating with acid or alkaline solution. The XRD patterns of the products with the ratio of 1.5Al/2Fe/2B calcined from 1130 to 1170 ℃ are shown in Fig. 2. $Fe_2AlB_2$ is the main phase with a bit of FeB and $Al_{13}Fe_4$ at 1130 ℃[14]. With the increase of temperature to 1150 ℃, these two byproducts are further consumed to form ternary boride and FeB almost disappears. For that of 1170 ℃, the peak intensity of $Fe_2AlB_2$ decreases dramatically, while those of FeB, $Al_2O_3$ and $Al_{13}Fe_4$ increase. It can be deduced that the ternary boride decomposes at higher temperature. The optimal reaction temperature is set to 1150 ℃ for this system. This method can be extended to the preparation of other ternary borides, and the related work is in progress.

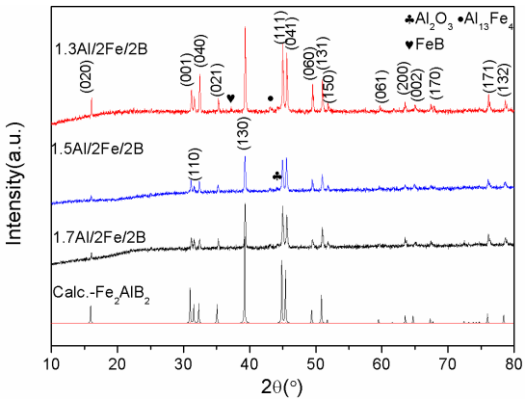


**Fig. 1. XRD patterns of products prepared from compacted raw materials at 1130 ℃**

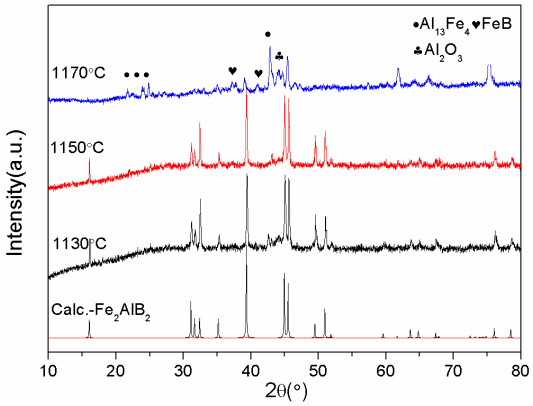


**Fig. 2. XRD patterns of products prepared from compacted raw materials of 1.5Al/2Fe/2B at different temperature**

The uncompacted reactants have been used for the synthesis as a comparison. The raw powders were directly poured into BN crucible for calcining after ball-milling. The reaction temperature was selected as 1150 ℃ and the ratio of Al content was 1.3 and 1.5, respectively. As shown in Fig. 3, Al and FeB are the predominant phases, while a small amount of $Al_2O_3$ coexists. There is no target product $Fe_2AlB_2$, even with various Al contents. It is noteworthy that there is no $Al_{13}Fe_4$, which as the important intermediate can react with FeB to yield ternary boride[14]. From a thermodynamic point of view, the reaction of Fe and B is easier than that of Al. However, this difference in reactivity can be overcome in the pressed green body, where the mass transfer distance is greatly shortened. When Al and Fe melt, they can infiltrate and combine with each other to form an alloy phase. Thus, the pre-compression step of raw materials is very important for the synthesis of $Fe_2AlB_2$. Such a feature is different from the well-known MAX phase, which can be synthesized from powdered reactants[15].

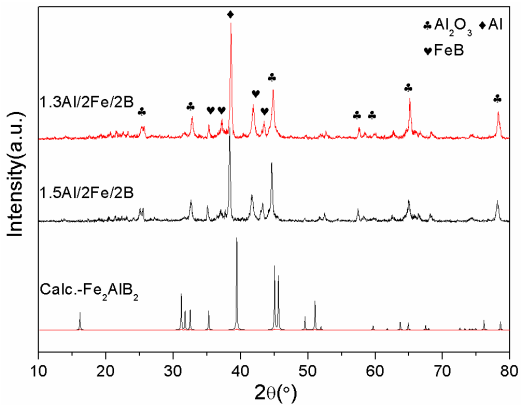


**Fig. 3. XRD patterns of products prepared from powdered raw materials at 1150 ℃**

In order to obtain $Fe_2AlB_2$ with high purity, the crude product was soaked in diluted HCl to remove the impurity phases. The effect of acid concentration and dwelling time on purification has been investigated. The grated product was treated with 1.0 and 1.5 mol/L HCl for 10 and 20 min, respectively. As shown in Fig. 4, $Fe_2AlB_2$ has totally decomposed into FeB, $Fe_2B$ and $AlB_{12}$ after etching by 1.5 mol/L HCl, although $Al_2O_3$ and $Al_{13}Fe_4$ have transferred into soluble $AlCl_3$ and $FeCl_3$. Under such high concentration, the dwelling time of 10 min also caused the decomposition similar to the 20 min process. When the HCl concentration is reduced to 1.0 mol/L, the impurities of $Al_2O_3$ and $Al_{13}Fe_4$ can be eliminated exactly. $Fe_2AlB_2$ also reacts with low concentration HCl but at a much slower rate, so $Fe_2AlB_2$ with just a trace of FeB can be achieved[16]. When the dwell time lasts to 20 min, the crystallinity decreases and a small amount of FeB and $Fe_2B$ appear. Therefore, the low concentration and short dwelling time are more advantageous, when HCl solution is preferred.

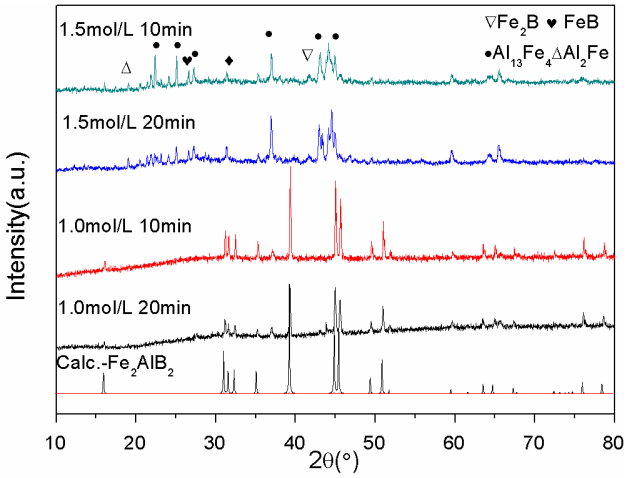


**Fig. 4. XRD patterns of products treated with HCl solution**

Alkaline solution can also dissolve $Al_2O_3$ and react slowly with iron and aluminum metals. In present work, the purification of crude product with NaOH solution is carried out and the effect of concentration and dwelling time is studied. As shown in Fig. 5, when the soaking time is 10 min, most intense reflections of the impurities between 40～45° disappears gradually with the increase of NaOH solution concentration. At the same time, a small diffraction peak appears around 37°, corresponding to the FeB phase. Furthermore, we fixed the NaOH solution concentration to 1.0 mol/L and adjusted the processing time (Fig. 6). When the etching time exceeds 20 min, all the impurity peaks disappear, and no iron boride phase exists. Therefore, low concentration NaOH solution with long immersion time has better results, which can effectively remove impurities and avoid decomposition of $Fe_2AlB_2$.

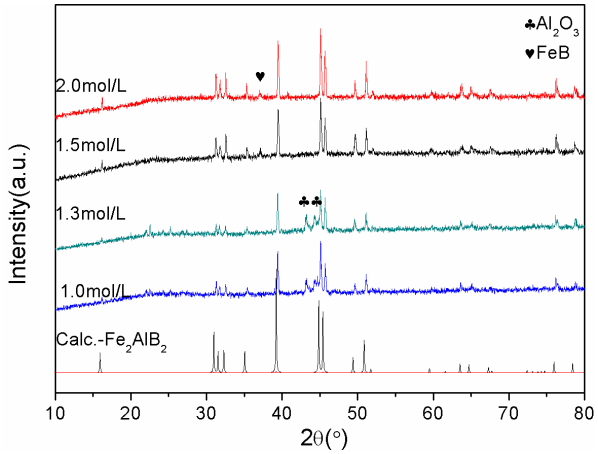


**Fig. 5. XRD patterns of products treated with NaOH solutions**

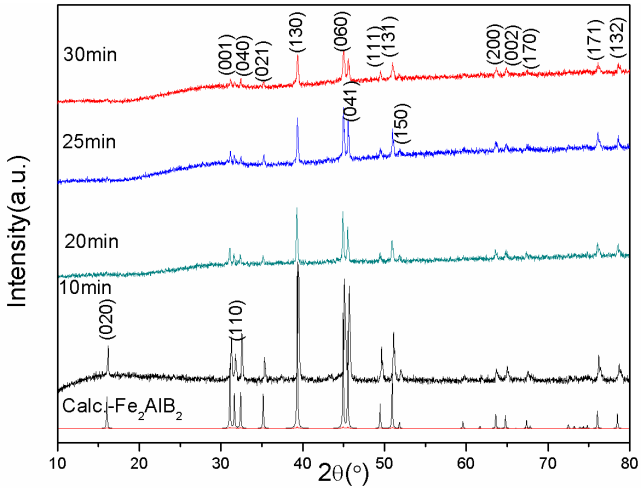


**Fig. 6. XRD pattern of products treated with 1.0 mol/L NaOH solution for different times**

### 3. 2 Thermal stability and microstructure of $Fe_2AlB_2$

The thermal stability of $Fe_2AlB_2$ has been studied in $N_2$ atmosphere (Fig. 7). The TG curve is stable before 150 ℃, after which the trace weight reduction (about 0.3 wt%) can be attributed to the volatilization of adsorbed water. The small amount of mass increase (about 0.4 wt%) between 200 and 1000 ℃ is due to the partial nitridation of Al component. As the temperature arises, the decomposition and nitridation of $Fe_2AlB_2$ increase, leading to a rapid weight increase, with a sharp endothermic peak at 1245 ℃. However, only 2% weight gains until 1300 ℃, indicating that $Fe_2AlB_2$ has good thermal stability and can be used as a potential high temperature material.

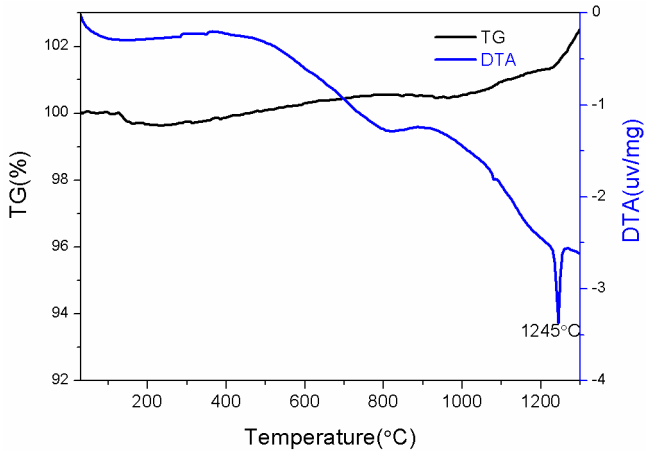


**Fig. 7. TG-DTA curves of $Fe_2AlB_2$ in $N_2$ atmosphere**

Previous reports mostly focus on bulk materials[17], while the micro-morphology of MAB powder has not been investigated yet. In the present work, a high-resolution observation of the ferromagnetic $Fe_2AlB_2$ powder is carried out for the first time, through the scanning electron microscopy (SEM) equipment with external objective lens. Fig. 8a shows the SEM image of as-prepared $Fe_2AlB_2$ powder with a particle size of 20～30 $\mu$m, where the irregular shape with obvious polyhedron outline can be seen. The grinding trace of the particle can be attributed to the weak basal planes, making it easy to damage during the milling process. The layered characteristic of $Fe_2AlB_2$ is illustrated in Fig. 8b, which can be explained by the crystalline structure, similar to those of MAX phases. After the treatment with NaOH solution, there is no obvious change in morphology, in which the polyhedron edges and laminated structure are still clear (Fig. 8c). This means that the reaction between NaOH and $Fe_2AlB_2$ is relatively mild, without destroying the microstructure. For the sample treated with HCl solution, the morphology changes greatly, where the particle size

decreases, the corners become round and the edges disappear gradually (Fig. 8d). The layers can still be observed, while the surface becomes rough with the attachment of fine particles. This can be attributed to the easier etching of Al atomic layer in the acid solution.

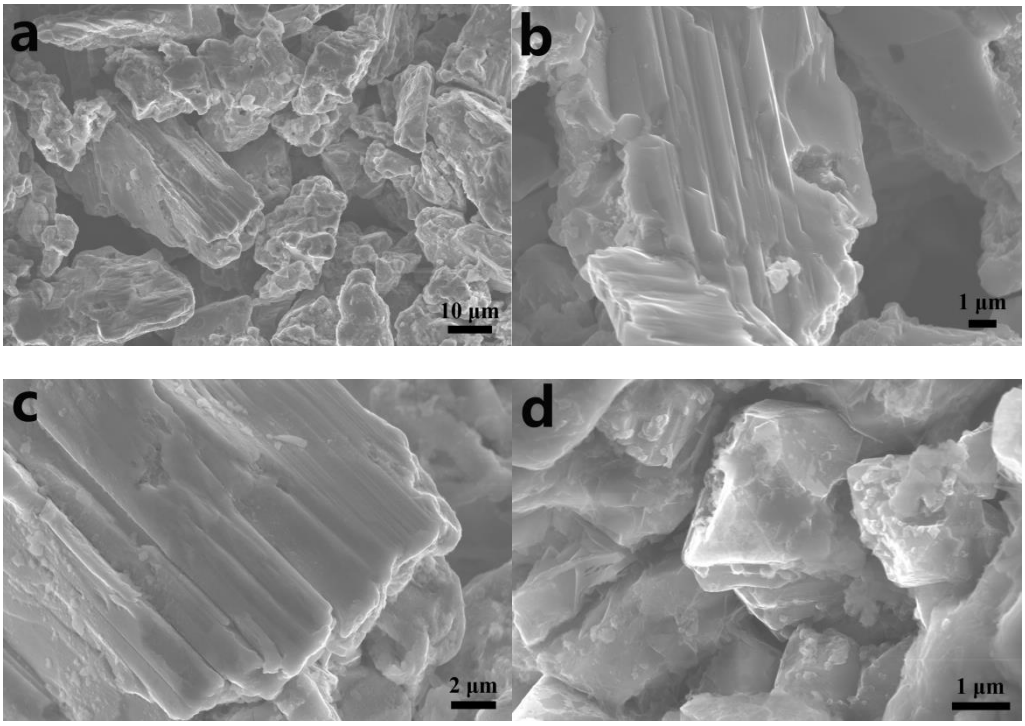


**Fig. 8. SEM images of $Fe_2AlB_2$. (a) and (b) As-prepared $Fe_2AlB_2$; (c) treated with NaOH solution; (d) treated with HCl solution**

### 3. 3 Composition, microstructure and properties of $ZrB_2$ ceramic sintered with $Fe_2AlB_2$

To investigate the effect of $Fe_2AlB_2$ as an additive on densification, microstructure and properties of $ZrB_2$ ceramic, the hot-pressing process at the relative low temperature (1250～1500 ℃) has been carried out. Fig. 9 shows the XRD patterns of the recants and as-sintered $ZrB_2$ ceramics with 25 wt% $Fe_2AlB_2$ at different temperature. The diffraction peaks of $ZrB_2$ are predominant, while those of $Fe_2AlB_2$ are not obvious, because the X-ray diffraction of $Fe_2AlB_2$ is much weaker than that of $ZrB_2$. As the sintering temperature increases, the diffraction intensity of $Fe_2AlB_2$ decreases with the appearance and increase of FeB phase. Because the $Fe_2AlB_2$ in the composite ceramic will decompose in a high temperature environment, in which the Al element was volatile, the FeB impurity in the composite ceramic at high temperature increases, while reducing the temperature, the MAB phase in composite ceramics increases. When sintering at 1500 ℃, $Fe_2AlB_2$ is almost completely decomposed. The composition of samples with different amounts of $Fe_2AlB_2$ sintered at 1250 ℃ is shown in Fig. 10. $ZrB_2$ is distinguished as the main phase, and several additional diffraction peaks are observed due to $Fe_2AlB_2$ and FeB, respectively. The $Fe_2AlB_2$ content in the raw material is proportional to the residual amount in the sintered body. Therefore, by adjusting the amount of additive and the sintering temperature, the phase composition of product can be modified conveniently.

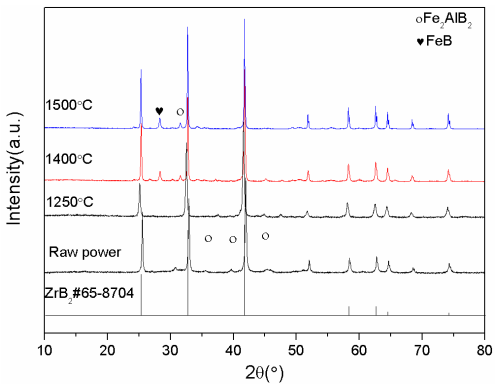


**Fig. 9. XRD patterns of $ZrB_2$-25% $Fe_2AlB_2$ ceramics sintered at different temperature**

The fracture surfaces of $ZrB_2$-25/30 wt% $Fe_2AlB_2$ sintered at 1250 ℃ are shown in Fig. 11. No obvious pores can be observed, confirming the high density. Besides the polyhedral grains, few layered components can be observed and identified as residual $Fe_2AlB_2$. $Fe_2AlB_2$ and FeB adjacent to $ZrB_2$ grains play an important role in joining and improve the

densification. The grain size tends to decrease with the increase of $Fe_2AlB_2$ content, which suggests the *in situ* formation of FeB and composition can effectively inhibit the grain growth. The fracture mode of monolithic $ZrB_2$ is dominantly transgranular, leading to the low fracture toughness. Due to the volatilization of the Al element in the high-temperature environment, the internal grains of the composite ceramic are rearranged. For present $ZrB_2$ with $Fe_2AlB_2$ additive, due to the different thermal expansion coefficients of $ZrB_2$, $Fe_2AlB_2$ and FeB, residual stress can be produced at the grain boundaries. When cracks appear, they tend to be deflected and to propagate along the grains rather than through them. Such intergranular fracture costs more energy to prolong the route expansion, so the fracture toughness of the material can be enhanced. In addition, according to the Hall-Petch relationship, the hardness and toughness could increase with the decrease of grain size due to the fine-grain reinforcing[18].

Table 1 summarizes the mechanical properties of $ZrB_2$ sintered with different amounts of $Fe_2AlB_2$. The increase of $Fe_2AlB_2$ composition can promote the densification of composite ceramics. When the mass fraction of $Fe_2AlB_2$ is 10%, the relative density is only 84.5%, and the presence of $Fe_2AlB_2$ can promote the sintering of composite ceramics. With the increase of additive, both the harness and fracture toughness have been improved. The high harness and fracture toughness of 22.3 GPa and 5.78 MPa $m^{1/2}$ respectively are obtained for $ZrB_2$ sintered with 35 wt% $Fe_2AlB_2$.

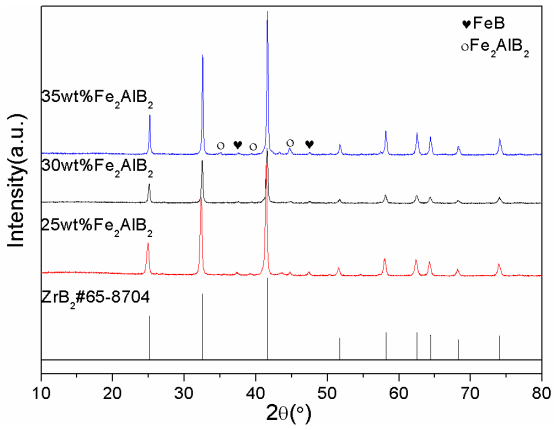


**Fig. 10. XRD patterns of ceramics sintered at 1250 ℃ with different $Fe_2AlB_2$ contents**

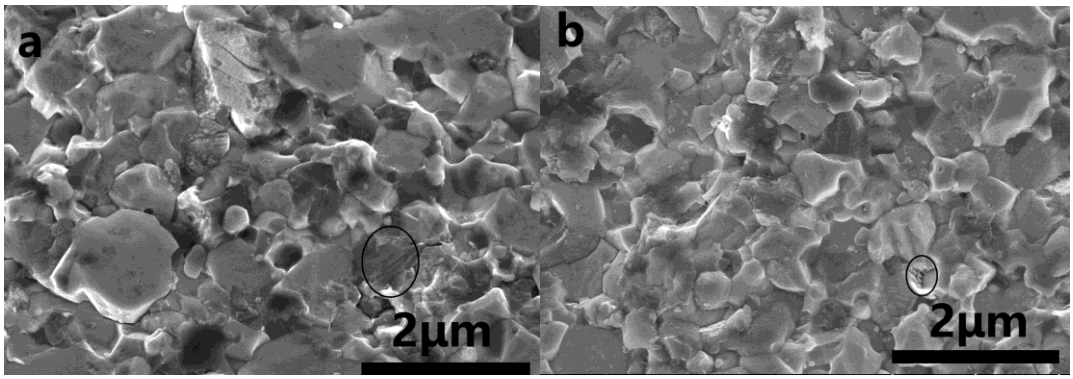


**Fig. 11. SEM images of fracture surfaces for ceramics with different $Fe_2AlB_2$ contents sintered at 1250 ℃: a 25 wt%; b 30wt%**

**Table 1. Mechanical Properties of the $ZrB_2$-$Fe_2AlB_2$ Ceramics**

| Material | Relative density (%) | Vickers hardness (GPa) | Fracture toughness (MPa $m^{1/2}$) |
|---|---|---|---|
| $ZrB_2$-10%$Fe_2AlB_2$ | 84.5 | 4 ±2 | - |
| $ZrB_2$-25%$Fe_2AlB_2$ | 96.0 | 18 ±0.6 | 4.64 ±0.2 |
| $ZrB_2$-30%$Fe_2AlB_2$ | 95.6 | 19 ±0.5 | 5.23 ±0.3 |
| $ZrB_2$-35%$Fe_2AlB_2$ | 96.2 | 22 ±0.3 | 5.78 ±0.5 |

## 4 CONCLUSION

$Fe_2AlB_2$ was successfully synthesized from compacted Fe, Al and B with molar ratio of 2:1.5:2 at 1150 ℃ for 30 min. The product was further purified by ultrasonic vibration in 1.0 mol/L NaOH solution for 15 min. Using $Fe_2AlB_2$ as a sintering additive, high dense $ZrB_2$ ceramics were obtained by hot pressing at low temperature (1250 ℃). Its relative density is up to 96.2 %, while the hardness and fracture toughness are 22 ± 0.3 GPa and 5.78 ± 0.5 MPa·$m^{1/2}$, respectively.

## REFERENCES


(1) Li, C.; Li, G.; Ouyang, H.; Lu, J. $ZrB_2$ particles reinforced glass coating for oxidation protection of carbon/carbon composites. *J. Adv. Ceram.* **2019**, 8, 102–111.

(2) Yu, Z.; Lv, X.; Lai, S.; Yang, L.; Lei, W.; Luan, X.; Riedel, R. ZrC–$ZrB_2$–SiC ceramic nanocomposites derived from a novel single-source precursor with high ceramic yield. *J. Adv. Ceram.* **2019**, 8, 112–120.

(3) Kavakeb, K.; Balak, Z.; Kafashan, H. Densification and flexural strength of $ZrB_2$-30 vol% SiC with different amount of $HfB_2$. *Int. J. Refract. Met. H.* **2019**, 8, 1–8.

(4) Shcherbakov, A. V.; Shcherbakov, V. A.; Barinov, V. Y.; Vadchenko, S. G.; Linde, A. V. Influence of the mechanical activation of reaction mixture on the formation of microstructure of $ZrB_2$-CrB composites obtained by electrothermal explosions under pressure. *Reractf. Ind. Ceram.* **2019**, 60, 223–226.

(5) Telle, R. The quasi ternary system $TiB_2$–$CrB_2$–$WB_2$ between 1900 and 2300 degrees C. *J. Eur. Ceram. Soc.* **2020**, 40, 341–348.

(6) Liu, H.; Zhang, X.; Peng, T.; Li, X.; Yan, Q. Preparation of large-scale $Ti_3SiC_2$ ceramic impeller with complex shape basing on the optimization of sintering manner. *Ceram. Int.* **2019**, 45, 22308–22315.

(7) Wang, Z.; Jiang, Y.; Liu, X.; He, Y. Pore structure of reactively synthesized nanolaminate $Ti_3SiC_2$ alloyed with Al. *Ceram. Int.* **2020**, 46, 576–583.

(8) Zhang, H.; Hu, T.; Wang, X.; Zhou, Y. Structural defects in MAX phases and their derivative MXenes: a look forward. *J. Mater. Sci. Technol.* **2020**, 38, 205–220.

(9) Liu, Y.; Ji, C.; Su, X.; Xu, J.; He, X. Electromagnetic and microwave absorption properties of $Ti_3SiC_2$ powders decorated with Ag particles. *J. Alloy. Compd.* **2020**, 820, 1–8.

(10) Wang, Y.; Wu, X. F.; Yang, Z. W.; Xia, Y. H.; Wang, D. P. Microstructure and mechanical properties of $Ti_3SiC_2$/$Ti_3SiC_2$ diffusion bonded joints using Ti foil as an interlayer. *Ceram. Int.* **2019**, 45, 20900–20909.

(11) Jin, S.; Su, T.; Hu, Q.; Zhou, A. Thermal conductivity and electrical transport properties of double-A-layer MAX phase $Mo_2Ga_2C$. *Mater. Res. Lett.* **2020**, 8, 158–164.

(12) Crisan, O.; Crisan, A. D. Incipient low-temperature formation of MAX phase in Cr–Al–C films. *J. Adv. Ceram.* **2018**, 7, 143–151.

(13) Niihara, K.; Morena, R.; Hasselman, D. P. H. Evaluation of $k_{Ic}$ of brittle solids by the indentation method with low crack-to-indent ratios. *J. Mater. Sci. Let.* **1982**, 1, 13–16.

(14) Liu, J.; Li, S.; Yao, B.; Hu, S.; Zhang, J.; Yu, W.; Zhou, Y. Rapid synthesis and characterization of a nanolaminated $Fe_2AlB_2$ compound. *J. Alloy. Compd.* **2018**, 766, 488–497.

(15) Dash, A.; Sohn, Y. J.; Va&en, R.; Guillon, O.; Gonzalez-Julian, J. Synthesis of $Ti_3SiC_2$ MAX phase powder by a molten salt shielded synthesis (MS3) method in air. *J. Eur. Ceram. Soc.* **2019**, 39, 3651–3659.

(16) Zhang, H.; Xiang, H.; Dai, F. Z.; Zhang, Z.; Zhou, Y. First demonstration of possible two-dimensional MBene CrB derived from MAB phase $Cr_2AlB_2$. *J. Mater. Sci. Technol.* **2018**, 34, 2022–2026.

(17) Li, N.; Bai, Y.; Wang, S.; Zheng, Y.; Kong, F.; Qi, X.; Wang, R.; He, X.; Duff, A. I. Rapid synthesis, electrical, and mechanical properties of polycrystalline $Fe_2AlB_2$ bulk from elemental powders. *J. Am. Ceram. Soc.* **2017**, 100, 4407–4411.

(18) Lu, S.; Li, X.; Zhou, Y.; Xu, W.; Ling, J.; Pan, W. Synthesis and mechanical properties of $TiB_2$/$Ti_2AlN$ composites fabricated by hot pressing sintering. *J. Ceram. Soc. Jpn.* **2018**, 126, 900–905.